

Explosives Detection and Analysis by Fusing Deep Ultraviolet Native Fluorescence and Resonance Raman Spectroscopy

Rohit Bhartia¹, William Hug², Ray Reid², Luther Beegle¹

¹ Jet Propulsion Laboratory/California Institute of Technology, Pasadena, CA

² Photon Systems Inc., Covina, CA

Correspondence: rbhartia@jpl.nasa.gov

1. Introduction

Raman spectroscopy of chemical, biological, and explosive (CBE) materials provides a high specificity means to determine whether an unknown material is a CBE compound, related to or is a precursor for a CBE, or is simply non-hazardous/non-threatening. During the last two decades advancements in lasers, electronics, optics, and miniaturized computing systems have enabled the development of compact Raman instruments that mobilize this capability from the lab to theater. However, even with these advancements, the traditional visible and near IR Raman instruments are still plagued with 2 major issues: 1) naturally occurring and material-related fluorescence emissions that interfere and obscure the Raman scattering and 2) an overall low sensitivity of the Raman measurement. Consequently, these two problems reduce the probability of detection and increase false negatives.

A solution to obscuration by fluorescence background and increased probability of false negatives is to use deep ultraviolet (UV) (<250 nm) excitation sources that enable a fluorescence-free Raman region and increases sensitivity to materials from Rayleigh and resonance Raman effects. However one of the more interesting results of using the deep UV is that the traditionally obscuring native fluorescence can be used as an orthogonal means of detection. Since the fluorescence is many orders of magnitude more sensitive than Raman and resonance Raman, it acts as a means to increase the sensitivity and probability of detection. While the probability of false positives may be higher, coupling the native fluorescence with deep UV Raman allows for both rapid searching over large areas, a means to down-select areas of potential concern and the use of the Raman effect to provide the high specify – a search analysis not possible with traditional visible and near IR Raman spectrometers.

This chapter focuses on explosives detection using the combination of deep UV native fluorescence and Raman spectroscopy using deep UV sources that enable compact, low power consuming devices. This includes a discussion of the deep UV lasers that are core to these fused instruments, a discussion of the deep UV Raman/fluorescence spectra using these compact deep UV laser, and a discussion of how the fusion of fluorescence and Raman enables a rapid, high sensitivity, high specificity analyses of explosives on surfaces.

2. Review of Deep UV spectroscopy for Explosive Detection

2.1. Explosive Detection Overview

“ What are you looking for, what level of information is required, and how do you intend on looking for it?”

These are questions commonly asked in the NASA planetary science community when determining what payload a mission to another planet will carry and provides the *Target, Required Information Content, and Concept of Operations (ConOps)*. For example, given the prevalence of perchlorates in the Mars soil, any instrumentation for organic detection and characterization that ingests and processes samples via heating or aqueous methods will not be ideal. In a similar manner, detection of explosives using instrumentation that requires direct contact to the material and/or suffers from ambient light rejection or background interference from the explosive material, is not appropriate for explosive detection.

The intent of an active spectroscopic method is to illuminate or excite a target to perturb the chemical structure in a manner that leads a detectable and uniquely identifiable response. As such, excitation of a target with a given wavelength of light leads to a variety of spectral responses including reflectance/absorption, Raman scatter, fluorescence, and in some cases, phosphorescence; each providing information specific to the chemical structure. The wavelength of light can affect both the presence and intensity of each type of response. For instance, observing the entirety of the fluorescence spectrum of single aromatic ring compounds requires an excitation wavelength of < 260 nm and, while Raman scattering is technically independent of wavelength, peak intensities can vary as a function of wavelength especially when considering resonance effects. With all of the possible spectral options and the benefits and challenges that each one faces, there is no one detection method that fits all detection scenarios. It is imperative that the instrument designs, capability, and *implementation* fulfill the needs of the explosive detection community. The goals stated below are high-level perspectives for Targets, Required Information, and ConOps.

Target: The technique needs to detect a variety of explosive materials including military grade explosives as well as materials used for Improvised Explosive Devices (IEDs) either made from military grade materials or are homemade materials (Homemade Explosives -HMEs). This also requires that the sensitivity to the targets is aligned with the ConOps.

Required Information Content: While the specific level of information are dependent on the exact nature of the ConOps, a thread common to this is determination whether a material is an explosive, a precursor, or a component to an explosive device. In all cases, the detection method needs to fit the required false positives and false negative requirements of the ConOps.

Concept of Operations (ConOps): This requirement is perhaps the most elusive as it is in some manner dependent on capabilities of available technology. However some level of common sense can be applied to this. An ideal *warfighter-level system* would include a compact, low system-mass, rugged, non-contact means of detection from some standoff distance, preferably one that extends to a range outside the hazard zone of a potential device, can operate under ambient light conditions, can handle a wide array of surface types, simple to operate and enable rapid method of detection from bulk to trace concentration of materials. Systems that operate at the *checkpoint-level* may allow for larger, less compact instrumentation, but would still require rapid detection of trace concentrations in ambient light conditions and detection on a variety of surface types. All off these however, also require that the detection method will not initiate detonation of a potential device and will not be hazard to the user or civilians.

As of yet, to the knowledge of the authors, no current instrument fits all of the requirements. Some systems, based on 1064, 785, and 532 nm laser-based Raman methods, provide part of the solution and have been very effective in introducing the potential of Raman spectroscopy for explosive detection [1]-[3]. However, while compact and potentially useful for a warfighter-level, there are limitations from an implementation/use perspective that includes sample-burning, obscuration of Raman signals from background fluorescence, and challenges with detection in ambient light conditions. This is not an issue with the specifics of the instrumentation design, but simply the challenges of operating in the near infrared (NIR) on the target materials of interest and in environments and operation parameters associated to the ConOps. This is also an issue with UV to visible Raman spectroscopy that includes excitation wavelengths ranging from 263, 266, 325, 405, 448, 532 and 633 nm. While ambient light does not obscure Raman scatter collected at 263 and 266 nm, the background fluorescence does still pose a significant problem.

Deep UV spectroscopy, defined here as excitation at wavelengths <250 nm, provides a potential compact solution for explosive detection as it avoids the potential for sample burning, fluorescence obscuration, and ambient light challenges while providing increased sensitivity and specificity. However enabling this technology for field use has required both scientific and technological research and development ([4]-[13]. It is only after the advent of compact deep UV laser sources < 250 nm, technological developments in optics, and development of understanding on how best to implement these technologies, has deep UV based fluorescence and Raman instrumentation been demonstrated as a compact, accessible at low cost, and is moving from specialized laboratories to compact hand-held sensors with wide-scale production. The range of potential applications includes, but not limited to, explosive detection, chemical and biological detection, forensic analysis, space exploration, pharmaceuticals, and water quality.

2.2. Deep UV Lasers

Deep UV lasers with emission wavelengths below 250 nm have typically been complex in design, expensive, volumetrically large, with high power requirements. However pioneering research from the Asher group demonstrated unique benefits, such as resonance enhancements for organics and a fluorescence free Raman region, both features that capitalize on deep UV sources <250 nm [14]-[26]. These benefits were of particular interest to the resurrected NASA's Astrobiology program in 1998, soon after claims of life in the Martian meteorite (Alan Hills 83001), where there was an obvious need for new life detection methods. Fortuitously, in 1996, Photon Systems Inc. was developing a new, simple, low cost, compact, low power requiring, deep UV laser <250 nm (Figure 2.2.1) ([27]-[30]. It was the advent of these lasers coupled to high quality deep UV optics that has enabled a new generation of instruments [31]-[33]. More recently it has also been realized that the Raman spectral enhancements as well as the fluorescence features enabled by the deep UV, are highly applicable to chemical, biological, and explosive counter-terrorism efforts as well as microbial detection for contamination assessment. (Bhartia et al. 2006, Bhartia et al. 2008; Bhartia, Fries, et al. 2010; Bhartia, Salas, et al. 2010; Fries and Bhartia 2010; P. V. Johnson et al. 2011; Lane 2010).

The choice of excitation wavelength depends on the availability of lasers with appropriate deep UV wavelength, emission linewidth, and other performance features such as size, weight, power consumption and cost appropriate to a miniature, hand-held, or small robot-mounted sensor. Laser emission wavelength, output power or energy, and linewidth are the dominant criteria to enable the ability to measure Raman emissions

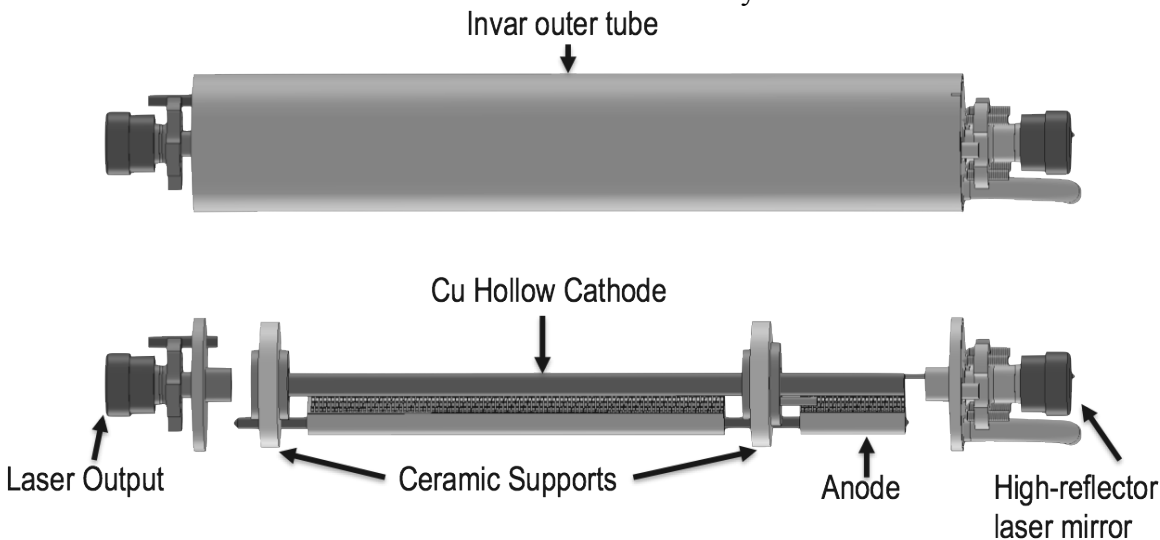


Figure 2.2.1. Schematic of Transverse Excited Hollow Cathode (TEHC) Neon-Copper (NeCu) laser (248.6 nm). The 224.3 nm, Helium-Silver (HeAg), has a similar construction where the Cu cathode is replaced by an Ag one. The robustness of the laser comes from its simplicity in design, tolerance to alignment, and no requirement of temperature sensitive components/materials.

from a target, and are the basis of an orthogonal Raman and fluorescence detection method. As illustrated above (Figure 2.2.1), lasers below 250 nm separate Raman and

fluorescence spectral regions for most materials of interest as targets or background materials and for the widest Raman shifts of possible interest.

Lasers which emit in the deep UV below 250 nm employ one of several basic technologies including: gas, solid state (including optical fiber), and semiconductors. Many government and internally funded programs have and are seeking to develop an “ideal” narrow-linewidth deep UV laser source compatible with both Raman and native fluorescence methods. Only two laser technologies provide *fundamental emission* wavelengths at wavelengths below 250 nm. These include excimer lasers such as krypton-fluoride (KrF) at 248 nm, krypton-chloride (KrCl) at 222 nm, argon-fluoride (ArF) at 193 nm, and fluorine (F₂) at 157 nm. In addition, there are transverse excited hollow cathode (TEHC) glow discharge lasers such as neon-copper (NeCu) lasers at 248 nm and helium-silver (HeAg) lasers at 224 nm. Wide bandgap semiconductor lasers such as aluminum-gallium-nitride (AlGaN) have sufficient bandgap to theoretically produce laser emission at wavelengths as low as 200 nm but have not yet demonstrated emission below 342 nm. All other lasers produce deep UV *emission using harmonic conversion* of their fundamental wavelength using non-linear optical crystals. Fundamental to the harmonic conversion process is the need for very high spectral radiance, measured in W/cm²/sr/nm. Second harmonic conversion efficiency is proportional to radiance in the non-linear crystal with second harmonic power being quadratically proportional to the fundamental source radiance. Typically a tradeoff is made in the crystal between acceptance angle and high power density is generated by strongly focusing the fundamental laser into the non-linear crystal. Power densities of hundreds of megawatts to per cm² are commonly needed to achieve reasonable conversion efficiency, over 30 to 50%. To achieve this in relatively miniature diode-pumped-solid-state (DPSS) lasers, peak power levels and pulse widths typically less than a few ns are required with consequences in sample damage. Continuous wave (CW) versions of harmonic generated deep UV lasers are typically very large, heavy, and have high power consumption.

Of the lasers described above, only the TEHC lasers have the size, weight, and power consumption to be compatible with hand-held instruments for proximity detection of explosives with the advantages of Raman and fluorescence using deep UV excitation. These lasers have excellent emission wavelengths at 224.3 nm and 248.6 nm, narrow linewidth less than 0.1 wavenumbers, weigh less than 2 pounds, including drive and power conditioning electronics and consume less than about 10 watts. Excimer lasers also have excellent wavelengths and can be made with narrow linewidths, but typically weigh about 50 pounds and consume over 50 watts of electrical power. As a result they are not compatible with hand-held sensor applications. CW laser such as argon ion lasers also have excellent wavelengths and narrow linewidths, but typically weigh over 100 lbs and consume over 10 kW of electrical power. The only lasers with the potential size, weight, and power consumption to be considered for hand-held sensors are 4th and 5th harmonic DPSS lasers. Unfortunately, the emission wavelengths of these lasers, at about 263nm or 266nm are not compatible with fluorescence-free Raman spectroscopy. Versions of DPSS lasers have been proposed at 236 nm and 228 nm, but

these have not been demonstrated in small, low power consumption, package sizes compatible with hand-held application.

The lasers employed for all of the Raman and native fluorescence results described here are Transverse Excited Hollow Cathode (TEHC) lasers. TEHC lasers have been under development at Photon Systems since beginning of full time operations in 1996. They are a unique type of laser, similar in construction to a miniature traveling wave tube or klystron, which provide direct CW transitions in the deep UV at 224.3 nm and 248.6 nm with peak output power over 500 mW. TEHC lasers have an emission linewidth less than 3 GHz, corresponding to less than 0.1 wavenumbers and emission wavelength stability better than 100 ppb, independent of ambient temperature. TEHC lasers have a high threshold for lasing and high slope efficiency. As a result, in order to reduce average power during operation, the input energy to the laser is commutated with a duty cycle typically less than about 1%. However since the transition is CW, a 30-100 μ s “long” pulse can be generated where the output energy in a typical 10 to 30 μ J with a long pulse. Comparatively, traditional pulsed lasers operate with pulse lengths of nanosecond or less creating very high peak power outputs that, consequently, can alter samples through heating.

TEHC lasers (figure 2.2.1) are about 30 cm long and 3.8 cm in diameter and weigh less than 1 lb. Average electrical power consumption is between about 1 W and 10 W, depending on pulse repetition rate, which is up to about 40 Hz in present configurations but have been demonstrated to operate at > 200 Hz. Because of the transverse excitation nature of TEHC lasers, 100s of mWs of deep UV output can be achieved in less than 10 μ s after application of electrical power at any ambient temperature from about -130C to +70C, without warm-up, heating, cooling, or temperature regulation.

Laser lifetime is presently between 10 and 50 million pulses, corresponding to 10 to 50 million spectra for efficient emitting target materials. Since these lasers have a virtual instantaneous warm-up, the lasers do not need to be consuming lifetime except when taking Raman or fluorescence data. This dramatically increases the effective field lifetime of these lasers compared to all other types of lasers. TEHC lasers are also unique in that they are, by far, the least expensive lasers of all lasers emitting in the deep UV below 300 nm.

In 2005, the U.S. Army independently rated Photon Systems’ TEHC lasers at TRL 5+ during a Technical Readiness Evaluation at Dugway, UT and currently under NASA being transitioned to TRL 6 for Mars applications. These lasers and related instruments and sensors have been on over a dozen major field expeditions in Antarctica, the Arctic, the deep Ocean, Death Valley, and other hostile environments as well as many other field trials and tests in real environmental circumstances. Recently, these TEHC lasers have been proposed as part of a deep UV fluorescence/Raman instrument for a multi-year surface rover mission to the planet Mars in 2020. In preparation for this mission, and development to TRL 6 for Mars, the lasers were repeatedly cycled at temperatures between -130 C and +70 C without failure. In addition, the lasers have been submerged

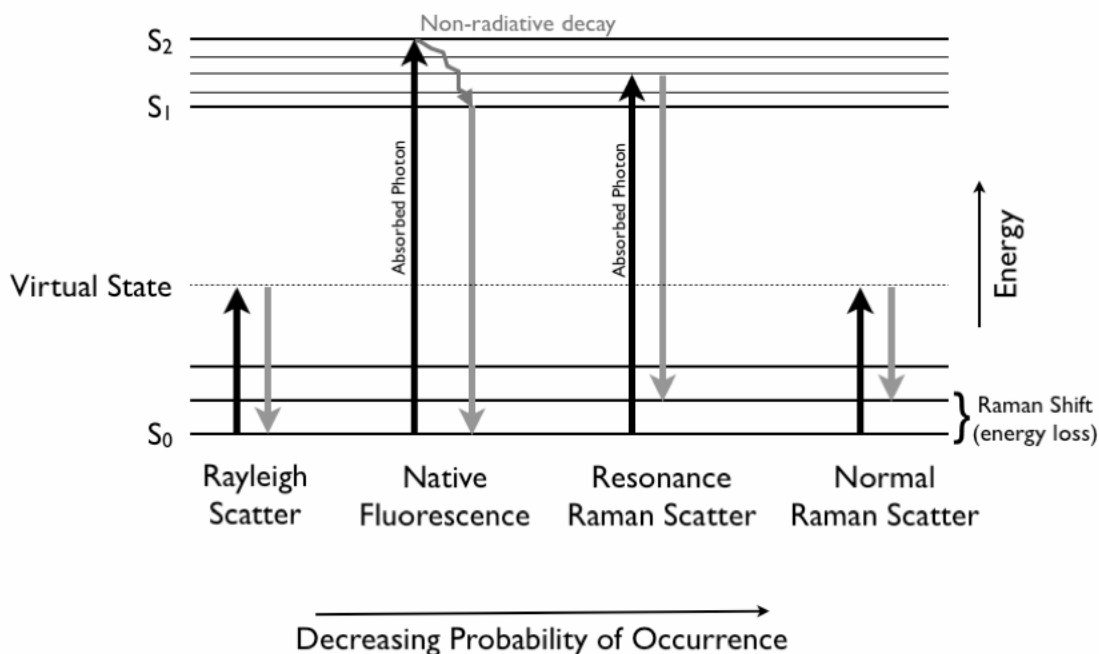
in liquid nitrogen, without failure. They have been tested to three times the shock and vibration specification for launch, cruise, and landing on Mars, without failure.

TEHC lasers achieve these performance characteristics by employing sputtering to generate the gain medium. In the case of the 224.3 nm HeAg laser, the gain medium is silver with a pump gas of a mixture of helium and heavier noble gas elements. In the case of the 248.6 nm NeCu laser, the gain medium is copper with a pump gas of neon. In both versions of these TEHC lasers, a glow discharge is generated within the hollow cathode via flutes in the cathode to a lateral brush anode. Radially inward 200 eV electrons generated at the inside surface of the cathode ionize and excite both noble gas atoms and ions, which in turn impact the cathode wall, generating metal atoms and ions to produce via charge transfer, the upper state population inversion needed for lasing. This process is fast, taking less than about 10 μ s, even from cold ambient conditions. This process is not dependent on ambient temperature or the heating of copper or silver to produce metal vapor. That is the reason these lasers can generate energetic states in the gain medium at extreme ambient temperatures without external heating and associated power consumption.

2.3. Deep UV Native Fluorescence Spectroscopy

2.3.1. Overview of Native Fluorescence

Native Fluorescence was first observed in 1565 from the extract of a medicinal wood, matlaline ([34]). Since then, the variety of compounds that are known to fluoresce is extensive. Most fluorescent compounds incorporate aromatic ring structures but there are some, such as acetone, that fluoresce without an aromatic ring [35]. In simple terms, fluorescence is the emission of a photon that *may* occur as an electron transitions from an excited state (S_1 - S_2) to a ground state (S_0). In most cases, this requires that a photon of a higher energy be absorbed by the molecule such that an electron can jump to the S_1 or S_2 state. Once excited into the S_1 or S_2 state vibrational energy levels consisting of vibrational, rotational, and molecular collisions cause the excited electron to non-radiatively lose energy until it reaches the lowest vibrational level of the excited energy state. This also includes an internal conversion from electrons in the S_2 state to fall to the S_1 excited state. The gap between the lowest energy level of S_1 and the ground state will dictate emission wavelength produced when the electron returns to S_0 . This emission can be heat or a photon that is less energetic than the initial absorbed photon. The wavelength of this emitted photon provides some information about the electronic levels that were available to the electron. Typically, as the physical size of the compound increases, there are more available vibrational states and the emitted photon is of a lower energy (longer wavelength); this is known as a Stokes shift. For example large sheets of graphene oxide



absorb the UV and emit at 600-700 nm while benzene, the simplest aromatic-ring compound, fluoresces at 260 nm [36]-[38]. These electronic transitions are best described using a Jablonski diagram (Figure 2.3.1). Phosphorescence is another light emitting event also described. This differs from fluorescence since the electrons undergo a spin transition to a T_1 level in a process called intersystem crossing. Conversion from the T_1 to S_0 also can result in an emission. This event is much slower than fluorescence

and can continue even after the excitation source is removed.

2.3.2. Advantages of Deep UV native fluorescence

In 2008, it was demonstrated that deep UV native fluorescence could detect and differentiate organics from a number of real-world backgrounds[36]. While the dataset at the time did not include explosives, it demonstrated that the excitation wavelength effected the ability to differentiate organics and that excitation <250 nm was optimal. The rationale behind this is a result of two main features (advantages) of operating in the deep UV (<250 nm): **Advantage 1) Observation of the full fluorescence envelope.** The fluorescence envelope can be considered as a convolution of a number of fluorescence compounds and includes organics structures such with aromatic compounds (benzene, naphthalene, anthracene, benzanthracene, etc), non-aromatic organics such as acetone, materials that are a composite of these compounds (microbes, mammalian cells, diesel

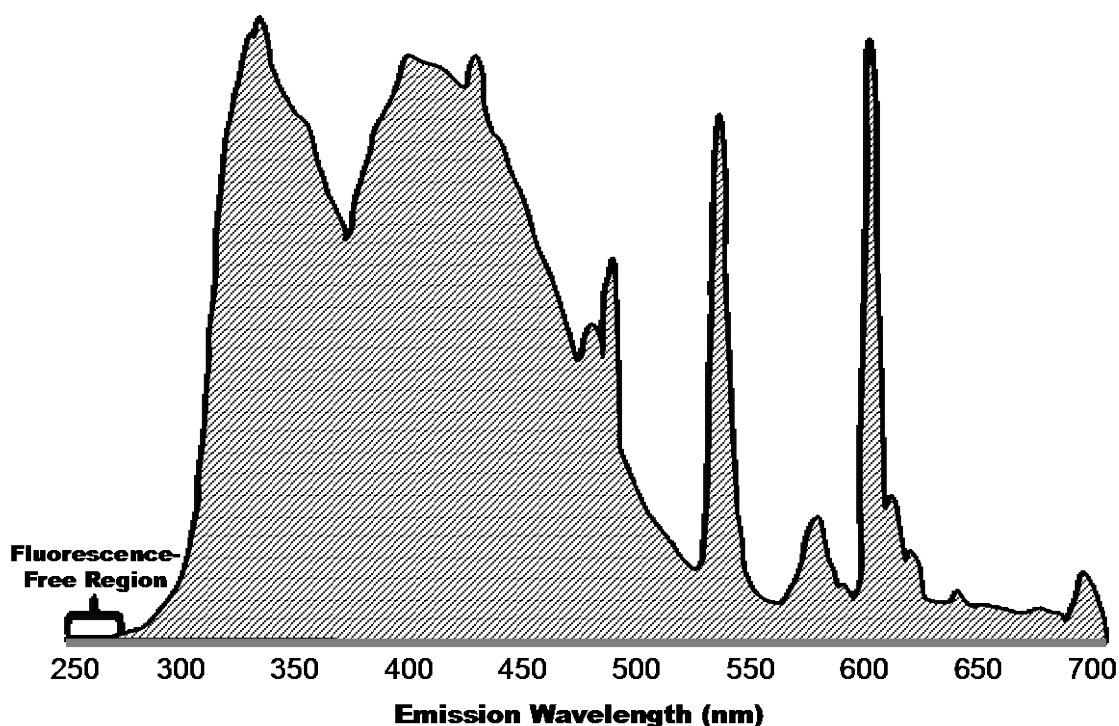


Figure 2.3.2. Native Fluorescence “envelope”. This data presented is an average of about 1000 naturally occurring materials (organics, microbes, minerals, etc). The excitation wavelength for all the spectra was 248.6 nm. This visually shows the fluorescence – free region <270 nm.

soot, gasoline, plastics, etc), as well as minerals that may fluoresce intrinsically or as a result of trace metals. An example of this fluorescence envelope is shown in Figure 2.3.2. To observe the entirety of a fluorescence spectrum, the excitation wavelength needs to be less than the minimum emission wavelength¹. As described in a number of papers, benzene, a single ring aromatic molecule, has some of the lowest fluorescence emission

¹ For the purposes of this discussion the authors are considering traditional fluorescence spectroscopy. However, there are some cases where this “rule” can be broken (Two-photon spectroscopy, antistokes emission from Photodissociation-Laser Induced Fluorescence (PD-LIF) etc).

characteristics with a lower emission wavelength at 270 nm [16], [18], [36], [39]-[41]. While advantage-1 suggests that use of a 270 nm an excitation wavelength is sufficient, advantage-2 explains why the optimal wavelength is actually <250 nm. **Advantage 2) Separation of fluorescence and Raman regions.** When illuminating a sample with a laser, a number of spectral phenomena occur nearly simultaneously; Rayleigh scatter, fluorescence, phosphorescence, Raman scatter, and of course heat. The Raman scatter, while rather weak compared to fluorescence, has some strong spectral features that can confound or interfere with the fluorescence spectra. While this sounds counter intuitive, it is becomes an increasing issue when considering trace detection. For instance, many organic hydrocarbons will have an intense C-H Raman stretching mode around 2900 cm^{-1} . Similarly an O-H stretching mode from materials in solution or compounds with hydroxyls will appear around 3400 cm^{-1} . If the background material such as plastic or water is present, these spectral features will confound low intensity fluorescence features from trace target materials. With an excitation line of 270 nm, these two spectral features appear at 292 and 297 nm respectively, well within the spectral range of a number of single ring aromatic compounds that constitute potential targets. While the Raman shift (energy loss) is identical for any excitation wavelength, using an excitation at 248.6 nm will shift these vibrational modes to 267 and 271 nm, allowing for a clear separation of Raman and fluorescence features, and avoids confounding either spectral phenomena.

2.3.3. Explosives with Deep UV Native Fluorescence

Targets

When considering *target* materials of explosives, there are two groups, *Military Grade explosives* and *Homemade Explosives (HMEs)*. These both can operate as Improvised Explosive Devices (IEDs), however HMEs use common materials in unknown concentrations and are more challenging to detect [42]. The source of fluorescence features of military grade active components such as trinitrotoluene (TNT), cyclotrimethylene-trinitramine (RDX), pentaerythritol tetranitrate (PETN) and octahydro-1,3,5,7-tetranitro-1,3,5,7-tetrazocine (HMX), have been limited to a few studies. Some of the early work on luminescence of RDX and HMX suggest a fluorescence emission associated to charge transfer occurring in the solid state [43]. In the Marinkas report, it was suggested that the fluorescence emission is centered at 465 nm at room temperature and is a result of a condensed state where charge-transfer effects are possible. In a more recent report from Sandia National Labs, the position-to-position fluorescence variability for a variety of explosives led to the conclusion that the fluorescence was a result of photo degradation products such as toluene (for TNT) or a result contamination [44]. Other reports suggest that 248 nm excitation of RDX will lead to fluorescence emissions from nitrous-oxide (NO_2) and hydroxyls (OH) [45]. However, these experiments used either high-peak power nanosecond pulsed sources, used sources in the *near UV*, and/or had limited spectral emission ranges. More recently fluorescence data of RDX, TNT, and PETN acquired using low-energy 248.6 nm laser (NeCu), with no more than 50 mJ/cm^2 at the sample show similar, featureless spectra in the 400 nm range but highly consistent for each sample. The maximum emission of RDX appears to be closer to 433 nm and observations at various locations show identical spectral features; suggesting that the fluorescence may not be associated with contamination but more likely the charge-transfer processes that Marinkas states. The primary band in TNT is 437 nm and again

suggests that minor spectral variations between these materials are consistent with charge-transfer features [43], [46]. However, it should be noted that these emission features are not intense but the fluorescence is still ~100x more intense than the deep UV Raman response. Furthermore, explosives that use the active components (RDX, PETN, HMX etc) in a composite matrix (C4, PE4 (Plastic Explosive 4), or Semtex) contain plasticizers, binders, dyes, and antioxidants that do have a strong fluorescence features. The antioxidants in particular are an integral part of the stability of these explosives and contain base aromatic structures [47]. Semtex for instance uses the same antioxidant (N-phenyl-2-naphthylamine) for all three version of Semtex. While this is a common antioxidant used in rubber production, the interaction between it and active energetic components such as PETN and RDX lead to a unique and differentiable fluorescence signature. This composite effect is similar to the fluorescence of microbes using deep UV native fluorescence [36] where the emission spectrum is a unique combination of fluorophores (aromatic amino acids) and absorbers.

Compared to military grade explosives, materials used for HMEs are quite varied and many of the components that are integral to the development of the explosive or the explosive end-product can provide significant fluoresce emissions. As with all explosives, there is an oxidizer and a reducing component. For example, in ammonium-nitrate-fuel-oil (ANFO) explosives, the ammonium nitrate is the oxidizer and the fuel-oil is the reducing component. While the ammonium nitrate is not natively fluorescent², the fuel oil, comprised of a variety of hydrocarbons including aromatic compounds, provides a highly structured fluorescence feature. As with the antioxidants fluorescence in military grade explosives, when fuel oil is mixed with ammonium nitrate, the fluorescence emission is altered from what would be with the fuel-oil alone. This also applies to perchlorate bombs where fuel oils are also used.

In addition to detecting the final explosive product, native fluorescence can be used to detect components used in forming HMEs. For example, TATP (triacetone triperoxide), a highly unstable explosive commonly used in HMEs, begins with acetone and hydrogen peroxide, where the former is fluorescent when excited at 248 nm. While it has no aromatic ring structure, acetones electronic states are structured such that they provide a unique fluorescence feature [35], [48], [49].

Fluorescence Information Content

² Similar to RDX and HMX the condensed state appears to have a charge transfer “luminescence” features. This has not been verified and is an area that requires further assessment.

In addition to detection of explosive materials either through primary phenomena or secondary one (i.e. a photodissociation effect) is necessary it is equally important to assess whether the response can be used to differentiate explosives from materials in the environment. In the case of fluorescence, the goal is to “classify” the material as hazardous or likely hazardous. Given the broad spectral features associated to fluorescence, this is a more attainable goal compared to identification. To understand the classification potential, the fluorescence spectra of explosives and other naturally and man-made materials can be analyzed by multivariate methods such as principal component analysis (PCA). This method offers a rapid means to determine whether any spectral features can be used to isolate or uniquely identify target materials; i.e. how unique are the explosive related spectral features detected by fluorescence. The traditional PCA model for fluorescence observed from 270 nm to 400 nm will separate materials based on their aromaticity (number and arrangement). A second order effect separates small aromatic compounds based on how they may be functionalized (hydroxylated (-OH), methylated (-CH₃), chlorinated (-Cl), aminated (-NH₃),

Fluorescence Analysis

Excitation: 248 nm/ PCA Analysis

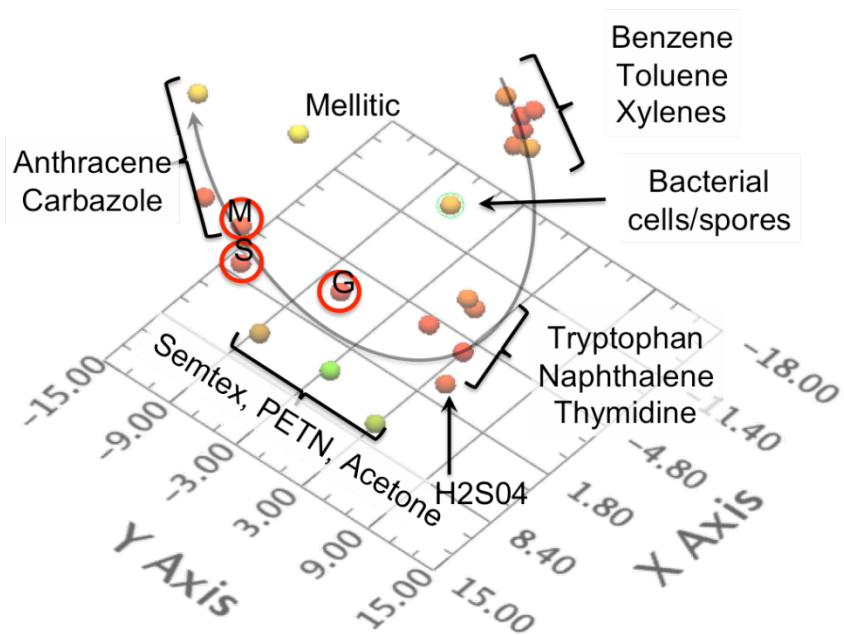


Figure 2.3.3. Fluorescence information content. Fluorescence analysis of the 27 samples that include explosives and components used to develop explosives compared to the organics and materials found in an operational environment. The excitation wavelength was 248.6 nm (NeCu laser). (Figure adapted from Bhartia et al. “Improved Sensing Using Simultaneous Deep UV Raman and fluorescence Detection”, 2012)

carboxylated (-COOH), etc) [36]. The PCA plot should place materials in “groups” with similar spectral features near one another. It should be noted that PCA is not a cluster

analysis method, however samples that group have spectral commonality that can assist in explaining what chemical feature (or component for composite materials) causes it to occupy a particular PCA position. For instance an organic such as benzene compared to a bacterial spore (containing dityroine), should be closer than chemicals like benzene and anthracene (one ring versus 3 ring aromatics).

Figure 2.3.3. shows a PCA plot of 27 samples using native fluorescence spectra excited at 248.6 nm using the Photon System's NeCu laser [8]. The grey arrow describes the overall trend line of aromaticity, beginning with benzene (1-ring aromatic) to anthracene (3-ring aromatic). Other samples in the database follow this line and in the majority of cases is a result of the aromaticity of the material. Composite materials such as bacterial cells and spores are not only separable but appear between the components that drive their fluorescence. Similarly, explosive materials such as Semtex appear between 2-ring compounds (naphthalene) and 3-ring compounds (anthracene). This is likely a result of the two overlapping fluorescence sources – the fluorescence of the antioxidant and PETN and/or RDX charge-transfer effects. PETN also appear near Semtex, but as it does not include the antioxidant features, it is not grouped with Semtex but since it is close spatially, it shows relatedness. Figure 2.3.3 also show where that acetone appears in the region nearby the PETN and Semtex. This begins to suggest that there may a spectral “region” that is common to explosives (see section 2.5 for a more complete analysis using a wider array of explosives and interferrants). As the dataset is by no means comprehensive, it is possible that non-explosive materials may appear in this “explosives region”. However it does demonstrate that native fluorescence spectral features of explosives, whether from antioxidants in the sample or the result of condensed state charge-transfer, can be used to differentiate a number of explosives from a wide array of organics and materials found in an operational environment. For example, preliminary analysis of explosives on a variety of surfaces including car panels demonstrated that native fluorescence was capable detecting and differentiating explosives from potential interferents such as Arizona road dust [7].

Fluorescence ConOps

The spectral features of explosive materials and the information content that deep UV native fluorescence provides, enables a “search and verify” concept of operations. Another way of describing this is that native fluorescence can be used to reduce the search area for slower and/or less sensitive but more specific detection methods like deep UV Raman. This conops leverages the benefits (sensitivity, speed, standoff distance) of the native fluorescence methods with some of the challenges (specificity).

From the perspective of a warfighter-system, a compact, standoff, handheld fluorescence system can be easily envisioned. Unlike high-resolution requirements for Raman, the broader features of the fluorescence require a spectral resolution of no greater than 1-3 nm and in many cases 10-20 nm bands are sufficient [50]. With this type of instrument, the warfighter would be able to enter an area, either indoors or outdoors, in any normal ambient light environment³, rapidly scan areas of interest compare spectra with an

³ This assumes that the spectral range observed by an instrument is <400 nm where direct sunlight during a 60-100 μ s laser pulse over the illuminated area would lead to a negligible amount of ambient background.

internal database and determine whether any features correlate to a spectral regions that contain explosive materials or components used to develop explosives. However, an instrument that used native fluorescence alone would require a secondary system to verify whether the detected feature is a potential hazard. Fortunately, one of the benefits of deep UV spectroscopy is that fluorescence and Raman spectral features can be collected using a single instrument without significantly increasing the size, power requirements, or complexity of the instrument.

With a checkpoint-system, native fluorescence enables reduction in the number of areas to target and also extends the detection to a further standoff distance, without the hazards typically associated to higher powered lasers. This enables a means for early detection and preparation for a potential threat. Again, integrating native fluorescence to deep UV Raman would allow for verification and identification of the explosive materials as a vehicle, object, or person approaches.

In both scenarios, it is imperative that native fluorescence spectral databases continue to develop and maintain traceability such that they can be integrated to onboard spectral libraries. These databases need to include not only the military and HME grades of explosive materials and precursor components but need to include materials from the operational environments. As these grow, newer more advanced algorithms can be developed to increase the certainty of detecting explosives while reducing false positives.

2.4. Deep UV Raman Spectroscopy of Explosives

2.4.1. Overview and Advantages of Raman and Resonance Raman

The Raman scatter effect is an inelastic scattering event first noticed by Sir C.V. Raman in 1928 [51]. For his discovery, he was awarded the Nobel Prize in Physics in 1930. Unlike Rayleigh scatter, this effect occurs when the illuminating photon interacts with bonds in the molecule and loses a small amount of energy defined by the bond. The stretching, bending or breathing motion and the atomic nature of the bond causes shifts in the returned scatter light. This shift in the excitation energy is independent of excitation wavelength [51] and is measured in terms distance from the excitation energy in terms of wavenumbers (cm^{-1}). The excitation energy, independent of wavelength is zero and the effect of this light interacting with a polarizable bond is described as energy lost from the excitation wavelength. Bonds such as the C-H stretching mode have an energy loss of 2990 cm^{-1} ; this will be the amount of energy lost from the incident source, irrespective of the excitation wavelength.

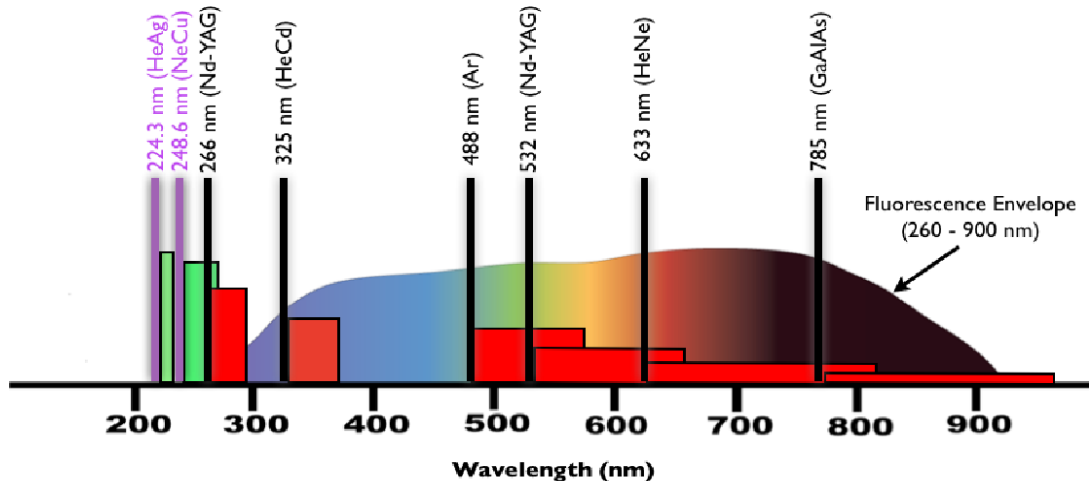


Figure 2.4.1 Raman Regions and Fluorescence Envelope and Available Lasers

Sources Each vertical line represents the location of a variety of laser wavelengths from the deep UV (<250 nm) to the NIR (785 nm). The green or red boxes next to each line represent the Raman region for the laser wavelength line to the left of it - with increasing excitation wavelengths, the Raman region encompasses a larger wavelength span. The colored region extending from 260 nm to 900 nm is the fluorescence envelope that includes organic and mineral fluorescence. Only the deep UV Raman regions (excitation wavelengths <250 nm) have green boxes indicating that the Raman and fluorescence spectral regions are separate.

Figure 2.4.1 shows the Raman regions for various excitation wavelengths in wavelength space. Although the energy lost from the excitation wavelength is constant for a particular vibrational bond mode, since the energy per wavelength is lower with increasing wavelength, i.e. as you move from the UV to infrared the energy of the photon decreases, the wavelength shift for the same bond increases with excitation wavelength. As a consequence, the Raman region, nominally from zero to 4000 cm^{-1} , increases with

increasing excitation wavelength.

Raman scattering is fundamentally low efficiency phenomenon. Compared to fluorescence, Raman bands are many of orders-of-magnitude less efficient. While Sir C.V. Raman used narrow line emissions from a mercury arc lamp at 435.8 nm, and was able to detect faint lines from carbon tetrachloride using film [52], the advent of lasers has allowed researchers to incorporate high radiance narrow linewidth lasers that typically range from the visible (532 nm) to the NIR (785 nm). While the wavelength of the laser used does not affect the Raman shift of a particular vibrational band, the cross-section (intensity) is related to the excitation wavelength. Thus the band intensities change as a function of excitation wavelength. This is independent of the Rayleigh law effects and dependent on matching the excitation energy with the bond energy.

However, as the excitation wavelength decreases, the Raman scattering efficiency increases by the Rayleigh law which is dependent on $1/\lambda^4$. This states that the Raman cross-section (efficiency of the Raman scatter) of any Raman band is 20x larger at 248 nm than at 532 nm and 100 x larger than at 785 nm. The intensity of the typical Raman bands are defined by the following, simplified equation (1.1) [53].

$$(Equation 1.1) \quad I_R = (I_L \sigma K S) P C$$

where I_R = detected Raman intensity in a specific band (in photons), I_L = intensity of the laser (photons), σ = absolute differential Raman cross-sections in terms of $\text{cm}^2/\text{molecule}/\text{steradian}$, K = optical component efficiencies, S = solid angle of collection (steradians), P = the depth of focus, and C = concentration in $\text{molecules}/\text{cm}^3$. For this equation, the polarizability has been included as a part of the σ - term since these parameters are difficult to determine from first principles. This equation also assumes that the Raman cross-section is provided for a given wavelength whose energy (in cm^{-1}) is significantly different from the bond energy. However, when the excitation wavelength and the excited vibrational state become similar, the Raman cross-section is said to be in pre-resonance or resonance. The cross section is defined in the following equation (1.2) (Asher and C. Johnson 1985):

$$(Equation 1.2) \quad \sigma = A \cdot \nu_o (\nu_o - \nu_R)^3 \left[\frac{(\nu_e^2 + \nu_o^2)}{(\nu_e^2 - \nu_o^2)^2} + B \right]$$

where ν_R = the Raman frequency (cm^{-1}); ν_o = the laser frequency (cm^{-1}); ν_e = the frequency of the transition to the excited state (cm^{-1}), and A and B = constants. The parameters A , B and ν_e are adjusted to fit the curve to experimental σ versus ν_o data. When the difference between the laser excitation frequency, ν_o , and the frequency of the transition to the excited electronic state, ν_e , goes to zero, the Raman scatter cross-section in Equation 1.2 $[(\nu_e^2 + \nu_o^2)/(\nu_e^2 - \nu_o^2)^2]$ goes towards infinity. In practice the enhancements provide 100 to 1000x and in special cases, $1e6$ times gain in the expected Raman cross-section [16]. Just between excitation at 532 nm and 248 nm pre-resonance effects for the O-H stretching mode increases by 120x due to Rayleigh and pre-resonance. The Raman cross-section of water, including both Rayleigh and pre-resonance effects, is 570x between 785 nm and 248 nm. This states that detecting an O-H stretching mode with a 785 nm laser with 570 x more power than using a 248 nm laser.

Traditionally, Raman spectroscopy attempts to excite a sample using an excitation wavelength that is not in the absorption region of the molecule(s) of interest [51]. Avoiding an absorption region of the molecule decreases the potential for a fluorescence background that, considering the significant variability in cross-section, would obscure the Raman scattering signal. For many organics and biological materials, visible to NIR excitation wavelengths result in a fluorescence background and is a problem from both a detection and interpretation perspective [16]. Typically Raman scattering is 10^4 to 10^8 times less efficient than fluorescence. Therefore if any fluorescence occurs within the target molecules or surrounding materials it will overwhelm the weak Raman emissions. To minimize the fluorescence effects researchers employ solutions such as time gating to take the advantage of the response difference between Raman and fluorescence, or use an instrument design with a highly confocal optical design such that the collected light is limited to only the illuminated volume contributing to the majority of the Raman signal. While time gating has shown to be effective, the current complexity of the instrumentation (detectors and lasers) prohibits its use as a compact solution for either the warfighter or checkpoint systems. Confocal optics, while highly effective in the lab, are not designed to be ideal for field use where focus tolerant designs are imperative. Alternative methods to avoid fluorescence are to capitalize on excitation NIR to IR regions that access a low fluorescence region using 976 nm and 1064 nm lasers. These require the use of Fourier Transform spectroscopy to overcome the thermal noise found in IR detectors. However this comes at a cost for sensitivity, since Raman scattering follows the Rayleigh law, the Raman cross-section in the IR are more than 2 orders of magnitude lower. Unfortunately, increasing the laser power is not a solution since the potential of thermally altering/burning increases with higher laser power.

The more effective solution to avoid fluorescence is the deep UV (< 250 nm). As stated in section 2.3.2, excitation below 250 nm, can produce Raman scattering in a fluorescence-free or fluoresce-limited zone. For the majority of organics, mineral defects, conduction bands, etc. that contribute to typical fluorescence/luminescence backgrounds the emissions are greater than ~260 nm. This was further proven in many subsequent publications on deep UV excitation [33], [40], [54]-[56]. The access to new deep UV laser sources and optics capitalize on both resonance Raman effects and as well as a fluorescence-free Raman region.

2.4.2. Deep UV Raman of Explosives

Targets/Information Content

Driven partly by a number of new deep UV laser sources, including NeCu and HeAg TEHC lasers, in the past 8 years there has been an increase in the number of deep UV Raman related papers exploring explosive detection [4]-[8], [13], [57]-[59]. The realization was that deep UV Raman (excitation <250 nm) provides an increased sensitivity to explosives through resonance effects, without the concern of obscuration from ambient light or fluorescence features stemming from dyes, antioxidants, binders, aromatic hydrocarbons found in many military grade and homemade explosives, or surfaces. The research world quickly demonstrated that this enhancement was prevalent for most major explosive materials and many of the primary HMEs [4], [5], [57], [58]. Unlike native fluorescence, deep UV Raman directed detects the active energetic components such as PETN, RDX, TNT, as well as HME components such as NO_3

Parameter	Units	Lab Instrument	Next Gen System	Notes/Ref
Parameter 1: Material				
Explosive Material			PETN	
Fill Factor			100%	
Material Raman Cross Section	cm ² /band/molecule/sr		3E-27 (1294 cm ⁻¹)	Ghosh et al 2012
Parameter 2: Optics (Illumination/Collection)				
Collection Aperture	f-number	4.0	7.0	
Laser Photon Energy Deposited	J/cm ²	53	46	
Collection/Spectrometer Optics Throughput	%T	0.08	0.21	
Parameter 3: CCD Parameters				
Collected Photons Incident on Detector	photons/pix	227	542	
Spectrometer CCD		e2v - 42-10		
Detector Temperature	°C	-126	-35	
Integration time	s	30	10	
Total Noise (sqrt[Dc+RN ²])	e-	2	3	1
Signal Detected on CCD	counts	89	232	
Results:				
SNR		45	116	

Table 2.4.1. Deep UV Raman photon budget model for PETN using the 1295cm⁻¹ resonantly enhanced band. The model incorporates instrument performance from the laser flux at the sample to the CCD and calculates an SNR.

(nitrates), ClO₄ (perchlorates), ClO₃ (chlorates), etc. (see Table 2.4.2 for deep UV Raman bands for these materials)

Most of the laboratory experiments to date demonstrated these results using high-powered deep UV lasers. However, these are highly unlikely to be used for a warfighter-system. In addition most results use long integration time coupled to high numerical apertures (NA) (low f-numbers). While these establish factors such as the Raman cross-section, the obvious question that is posed is whether a more portable, compact, and ruggedized laser, such as the TEHC deep UV lasers can be used for resonance Raman explosive detection and enable a compact implementation that considers the warfighter. For reference, these lasers deposit 3-6μJ/60μs (50-100mW peak power) on the sample per pulse with a repetition rate of up to 40Hz. However beyond the compact size of the laser, the implementation for a warfighter requires that the systems f-number is high enough that the design is relatively focus tolerant; i.e. it will enable operation similar to a DSLR camera (Digital Single Lens Reflex camera) (simple and rapid autofocusing capabilities). This translates to an increased observational area with a decreased solid

Table 2.4.2. Deep UV Raman bands for a number of military and HME explosives materials

Primary Raman Bands (wavenumbers) with 248.6 nm excitation						
Military Explosives						
Trinitrotoluene (TNI)				1361		1624
Pentaerythritol tetranitrate (PETN)	872		1295		1511	1658
Cyclotrimethylene-trinitramine (RDX)		1025 1280		1381 1464		
C4 (RDX)		1025 1280		1381 1464		
Semtex (PETN+RDX)	872		1295	1381 1464		1624
Homemade Explosives (HME)s						
Nitrate		1044	1365			
Perchlorate	932					
Chlorate	935					

angle of collection– exactly opposite of the traditional method used for sensitive detection.

However, even with these limitations, high sensitivity detection is still feasible with these lower powered fieldable lasers – mainly a result of the increased Raman cross-sections in the deep UV. To understand this, a photon budget model considers the explosives targets Raman cross-section, optical collection and throughput, detector sensitivity and noise profiles, as well as the laser energy deposited on the sample (Table 2.4.1). The collection volume is stated as fill-factor, a term used to describe how much of the illumination beam diameter is occupied by the target material [60]. The Next Gen system column in Table 2.4.1 describes the SNR (Signal to Noise Ratio) with a TE (thermally electrically) cooled CCD rather than the lab standard liquid nitrogen cooled CCD and a larger f-number (f/7) and a shorter integration time. Both instruments employ shot-noise limited detectors where the dark noise is negligible at the required integration times. However, the reason for the observed difference in SNR between the two instruments is a result of an optimized coupling of the spectrometer and decreased magnification in the next-gen system.

Beyond the theoretical (Table 2.4.1), this has been demonstrated empirically with PETN, TNT, RDX, RDX, C4, and Semtex on using the 248.6 nm NeCu lasers (figure 2.4.2). In addition, HME relevant materials such as NH_4NO_3 , $-\text{ClO}_4$, ClO_3 , have also been demonstrated (figure 2.4.3). Both sets of data were collected on the lab instrument with a NeCu 248.6 nm laser (Photon Systems Inc.), with 53 J/cm^2 at the sample, using an f/4

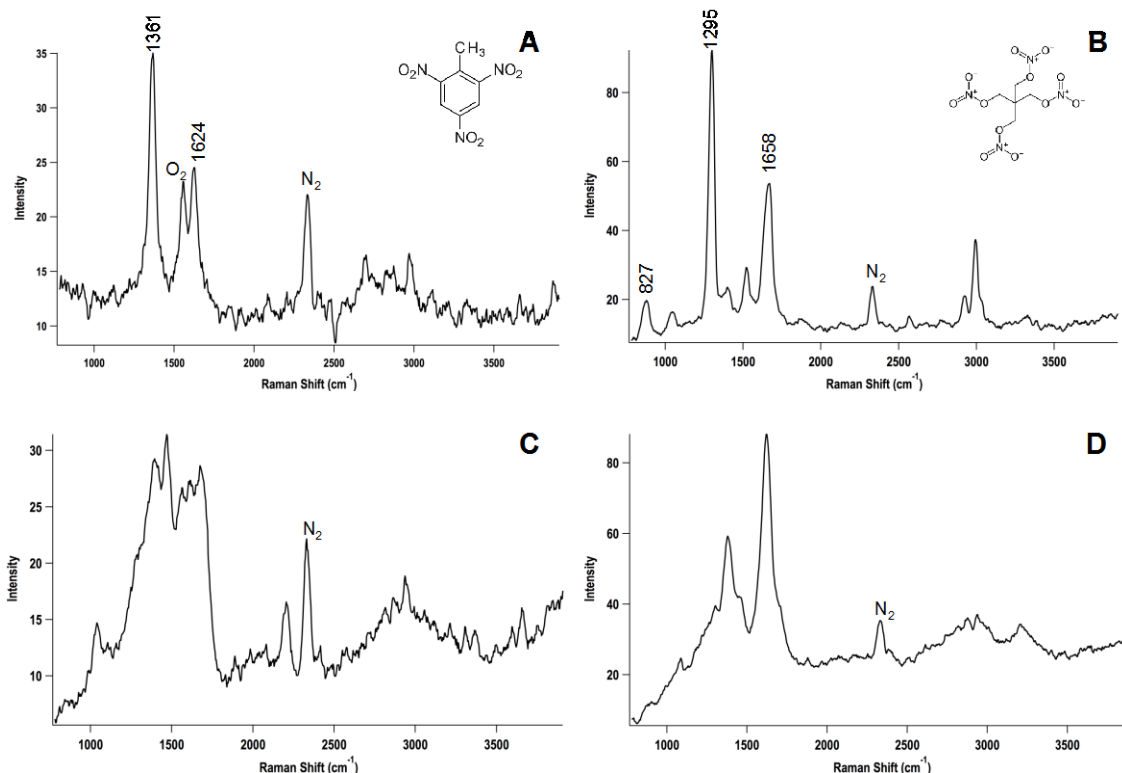


Figure 2.4.2. Deep UV Raman spectra of military grade explosives using a compact, ruggedized hollow cathode NeCu laser. A) TNT B) PETN, C) C4 and D) Semtex.

objective lens, with a 100% fill-factor and detector integration time of 30s. It should be

noted that the PETN data verifies the model and shows a 98% correlation between the estimation and actual data.

Visual comparison of the Raman spectra in figures 2.4.2 and 2.4.3 of military grade and HME related explosive materials shows that while the Raman cross-sections for TNT, PETN, C4, and Semtex are higher than the nitrate, perchlorate, or chlorate, the SNRs are inversely related. Since the data were collected with identical acquisition parameters, the relative signal strength can be compared using the intensity of the N₂ (air) line. In the military grade samples this band is apparent, while in the HME spectra it cannot be seen when plotted on the same scale as the primary Raman peaks. This appears to contradict the expectation that materials with enhanced Raman cross-section lead to decreased SNR. What needs to be taken into consideration is the actual interaction volume and the mass or number of molecules within the interaction volume. Comparing the molecular absorptivity's at 248 nm of nitrate, PETN, and TNT range from negligible, to 0.05, and 1.5 ($\times 10^4 \text{ L}\cdot\text{mol}^{-1}\cdot\text{cm}^{-1}$) respectively[4]. The resulting SNRs from the collected spectra are inversely related with SNRs of 1400 (nitrate), 44 (PETN), and 12 (TNT). This demonstrates that as the excitation wavelength decreases, the Raman cross-section may increase, but at some "cost" of a decreased interaction volume (i.e. a reduction in the volume of material from which the signal is detected). This effect is most obvious when looking at bulk samples where sensitivity appears low (low SNR). However, because of the material absorptivity it limits the number of molecules being observed, even in bulk. Therefore, linearly decreasing the concentration will lead to a non-linear decrease in SNR. *With highly-absorbing materials, bulk analyses do not lead to a determination of theoretical detection limits. Furthermore, highly-absorbing materials are more amenable to "trace detection" where materials are dispersed in a background matrix, or are a thin layer on background.*

To demonstrate this, an aromatic compound, phenanthrene was formed into three pressed-pellets at concentrations ranging from 100% to 0.1% (weight percent). One

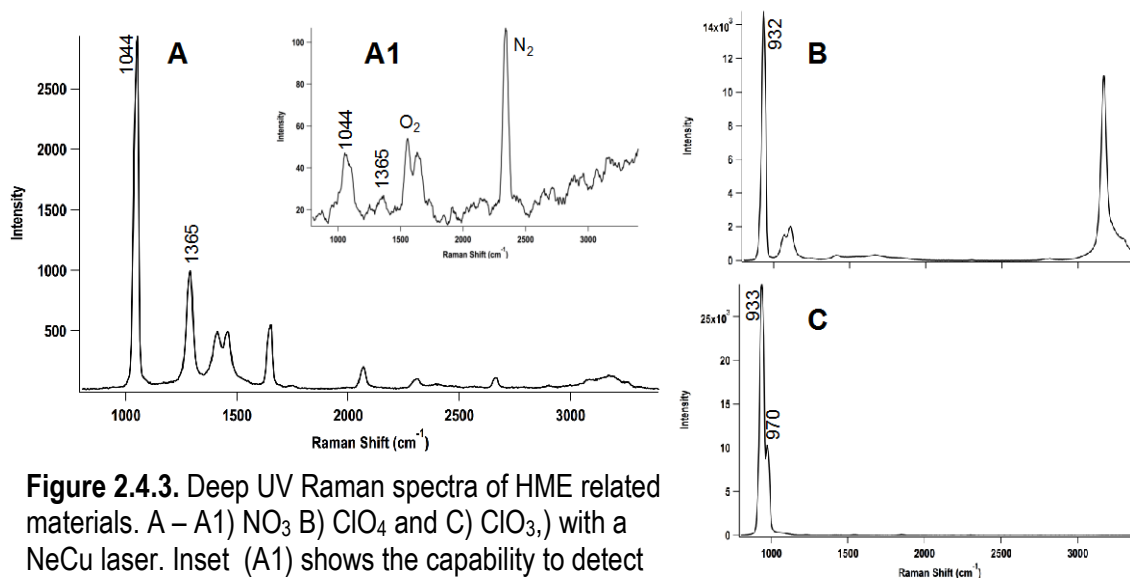


Figure 2.4.3. Deep UV Raman spectra of HME related materials. A – A1) NO₃ B) ClO₄ and C) ClO₃,) with a NeCu laser. Inset (A1) shows the capability to detect nitrates at 1% in basalt (natural environment).

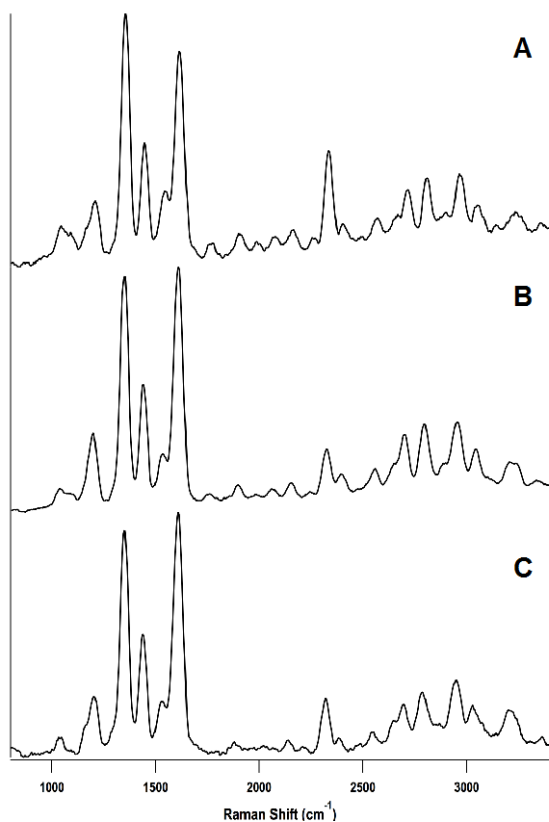


Figure 2.4.4. Bulk versus trace detection with materials high molecular absorptivity/advantage of resonance Raman. 248.6 nm deep UV Raman spectra of phenanthrene in pellets as pure (100%) and mixtures in naturally occurring basalt at 1% and 0.1%. A) 0.1% Phenanthrene + Basalt, B) 1% Phenanthrene in Basalt, C) 100% Phenanthrene pellet. The SNR for the pure material is 155, a 1% solution is 199 and the SNR for the 0.1% solution is only 92, i.e. a ~25% decrease in SNRs with order of magnitude decrease in concentration

percent and 0.1% solid-solid dilutions for the pellets were made in a naturally occurring basalt whose chemistry has been well established [61]. With a molecular absorption value of $\sim 1.3 \times 10^4 \text{ L} \cdot \text{mol}^{-1} \cdot \text{cm}^{-1}$ at 250 nm, phenanthrene's depth of penetration will be equal to that of TNT[4], [62]. The data collected (figure 2.4.4.) show deep UV Raman spectra where the SNRs are 155, 119, and 92 for 100%, 1% and 0.1% dilutions respectively. For weakly or non-absorbing species the SNRs should follow a linear plot. As shown in figure 2.4.3, the nitrate shows this linearity. Potassium nitrate was formed into pure pellet and a 1% mixture with basalt. In the pure pellet, a 100% fill factor, the SNR was 1400, while the 1% fill factor has an SNR of 22. The phenanthrene data however follows a natural log plot showing the effect of transmission of laser into the material. The depth of penetration with a 248 nm laser into pure phenanthrene can be calculated as 400 nm, resulting in a view volume of $\sim 2 \text{ pL}$, and an observable mass of phenanthrene of $\sim 2.3 \text{ ng}$. Previous efforts have demonstrated that the depth of penetration in the deep UV in basalt substrate is $>30 \mu\text{m}$. Therefore given the 23% decrease in the SNR with a 1% solution of basalt and phenanthrene, the mass of phenanthrene observed should be 1.7 ng and equates to a depth of penetration of $15 \mu\text{m}$. With a 0.1% solution the depth of penetration increases to $\sim 20 \mu\text{m}$ with an observable mass of 240 pg.

The phenanthrene dilution analysis demonstrates the benefits of resonance effects for trace detection but also highlights the non-linearity of as function of concentration. As a result high molar absorptivity's, the mass of material being detected, even in bulk samples are limited. The mass of observed material be extended by increasing the illumination beam diameter but traditionally there are negative ramifications to the instrument in terms of increased size or reduction in spectral resolution limits increasing

the beam diameter. Alternative spectrometer designs such as Spatial Heterodyne Spectrometers (SHS) may offer a means to increase the illumination area without these particular side effects and is an area of research and development [63]. *In the case of the instruments described here, the maximum observable mass is $40 \mu\text{g}/\text{cm}^2$. With a 6:1 SNR, the detection limits are $<1\text{ng}/\text{cm}^2$.* Comparatively, excitation wavelengths in the visible or NIR that are poorly absorbed by the material require a large quantity of material in their interaction volume and are not amenable to trace detection. Solutions to increase sensitivities with vis-NIR methods are to increase laser power that leads to thermal damage and potential fire hazards. Given that lower concentrations of particles more are likely a realistic scenario, the deep UV excitation offers unique advantages for performing both bulk and trace.

Deep UV Raman ConOps

As shown in a number of publications, deep UV Raman spectroscopy offers a high sensitivity method for explosives detection. However, until recently, this has only been demonstrated with laboratory instruments that would be difficult to transition into field deployable sensors for the warfighter. For checkpoint conops where power and size are less of an issue existing larger lasers have been implemented and been used to demonstrate the utility of the technology. However, as shown with the data above, warfighter conops can be enabled and the check-point-level conops can be enhanced by compact deep UV fluorescence/Raman devices enabled by these lower powered deep UV lasers. While the SNRs may not be equivalent to the laboratory systems, they are more than sufficient for trace detection and even enable detection with f-numbers that are amenable to handheld deployments. However, the deep UV Raman detection methods, as with all Raman based devices, observe small areas and require a secondary method, such as deep UV fluorescence, to reduce the search space/target deep UV Raman analyses.

2.5. Spectral Fusion: Benefits of Combining Deep UV fluorescence and Raman spectroscopy

In addition to operating as a means to search for potential explosives, the native fluorescence methods can be fused with the deep UV resonance Raman information to provide an orthogonal information set. Preliminary tests of the combined method have been successfully demonstrated on explosives, chemical agents, as well as planetary science. In effect the fluorescence method provides a separation based on electronic characteristics of the material (available energy levels), while the deep UV Raman provides the vibrational description of the material.

As stated in section 2.3.3, the majority of military grade explosive fluorescence features are a result of charge-transfer based fluorescence. While explosive materials are not the only class of materials that exhibit this feature, detection of this it does reduce the number of potential targets that would require analysis by deep UV Raman. Additionally, while the fluorescence spectra are not diagnostic for explosives, it can also be used to aid in reducing the number of samples in a Raman database classification step. This helps to resolve one of the challenges that Raman algorithms with large databases face. Although the details of these algorithms are proprietary, the basic concept typically compares the spectral features from an unknown sample to a database of samples previously acquired

on the instrument or on a master instrument. As the types of materials in the database increases, the features that enable differentiation begin to become increasingly difficult where resolution, stability (e.g., laser position), background suppression, and SNR become increasingly important to enable classification/identification. Any means to reduce the possible range of materials provides an advantage and can reduce the requirements of spectral resolution and enable detection and identification with lower SNRs.

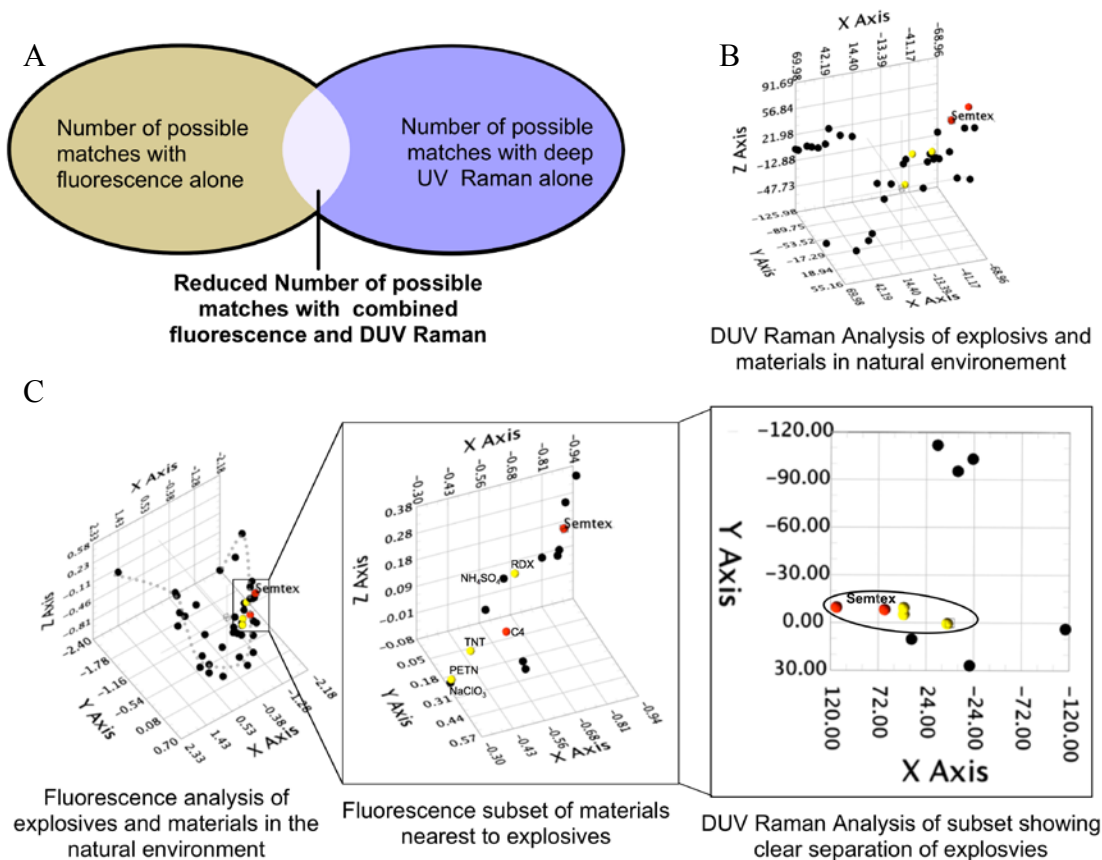


Figure 2.5.1. Improved detection with Deep UV Raman analysis preceded by deep UV fluorescence analysis. The ven diagram pictorially describes the benefit of combining fluorescence and deep UV Raman. Using either of the spectral phenomena alone requires differentiating an unknown material from a large numbers of possible materials (B - example Raman of explosives and common materials in the natural environment). By combining the two spectral features, the number of possible materials decreases (C). In this case, combining is an iterative process that begins with fluorescence to reduce the possible materials to a small subset, and then Raman analysis of the subsets. PCA was used for this analysis for simplicity and traceability to previous work. In C, the grey dotted line in the fluorescence analysis defines increasing aromaticity (single ring aromatic on the left). In all panels C4 and Semtex (labeled) are the red spheres and RDX, PETN and TNT are the yellow spheres. For the fluorescence analysis, explosive compounds appear in a cluster near 2-ring aromatic compounds. This region is extracted as a subset of the database and used for deep UV Raman analysis. Visual comparison between the methods shows grouping of the explosive materials are better in combined method (C).

Figure 2.5.1 graphically represents how the step-wise use of fluorescence followed by deep UV Raman compares to a Raman only approach. This analysis assumes that the material in question is Semtex. The database includes materials ranging from toxic industrial chemical (TICs) (xylenes, benzene, sulfuric acid, etc), biological material (bacteria, amino acids, plant material), minerals, polyaromatic hydrocarbons (PAHs), chemical agent analogs, as well as military grade and HME explosive materials. Using fluorescence, Semtex would appear in a cluster near 2-ring compounds, close to other explosive materials. The rationale as to why Semtex appears here is its antioxidant chemistry that contains a naphthalene base. However, natural materials that have no explosive relevant chemistry are also interspersed. It should be noted that this region appears to include spectral features associated to 2-ring aromatic compounds (such as naphthalene) and non-aromatic compounds that exhibit charge transfer –like fluorescence (or luminescence) properties in the condensed state. While these other compounds can lead to increased potential of false positives, in a potential ConOps, a warning can appear stating that further investigation is required at which point the area in question is targeted and deep UV Raman data area collected. However rather than comparing the acquired results to the entire database, the data are only compared to the subset of samples close to Semtex (in PCA-fluorescence space). The results of the subset analysis show an “explosives” group forming where it easily separated from the other non-explosive materials. Comparatively, if deep UV Raman alone were used, figure 2.5.1 shows how Semtex and other explosives (red and yellow spheres) are interspersed between biological compounds and non-hazardous components. Theoretically, by increasing this, the PCA space for the Raman only analysis would lead to increases separation of the materials, however it is likely that they will still remain interspersed. However, since the variability of position in this PCA space is dependent on noise and variability of the sample, the ability to clearly identify materials relies on high SNR; decreasing this would lead to increased false positives.

In both the fused fluorescence/Raman and the Raman only analyses, the deep UV Raman resolution was $\sim 45\text{cm}^{-1}$. The benefit of the fluorescence/Raman combined method, is the ability to detect (fluorescence), decrease false positives (fluorescence+Raman), and identify the sample (Raman). An added advantage to this is that the requirements on spectral resolution are decreased from the traditional $5\text{-}10\text{cm}^{-1}$ down to 45cm^{-1} , and are not reliant of high SNRs.

3. Current Capabilities and New and Emerging Efforts

As presented in the sections above, many of the instruments used to collect the data were laboratory instruments. However these were configured with the perspective of field deployments in mind. For example, the lasers that were used were the NeCu and HeAg deep UV sources from Photon Systems that are rugged, compact, and have low power requirements (<10W). In other respects, these lab instruments are the “gold-standard” and included low-stray light spectrometers with liquid-nitrogen (LN2) cooled detectors and a stable platform. As such they provided the ability to understand the potential of the compact deep UV lasers, and guided many of the resulting field instruments. As seen in figure 3.1, the deep UV instrument range from the laboratory gold standards (3.1.A) to compact thermoelectrically (TE) cooled versions for planetary science (3.1.B), to fluorescence and fluorescence/Raman scanners, standoff instruments, underwater systems, and microscopic systems.

As stated in the beginning, “*What are you looking for, what level of information is required, and how do you intend on looking for it?*” – these questions drive instrument design. As such, many of the deep UV field instrument developments were driven by questions in planetary science (figure 3.2). However, more recently, the field instruments, such as the Targeted Ultraviolet Chemical Biological Explosive (TUCBE) sensor have been developed for detection of chemical/biological/explosive from a standoff distance. While the details of the instrument design are outside the scope of this chapter, the TUCBE uses a 248.6 nm laser to illuminate target and collects both fluorescence and Raman emission with Dall-Kirkham reflective objective lens. The detection system splits the deep UV Raman and fluorescence paths into a dichroic stack with PMTs (photomultiplier tubes) for the fluorescence, and a grating spectrometer path with a 32-channel PMT array for Raman detection. This is considered a low-resolution spectral instrument, but what it provides is a rapid solution to detect materials using the combined fluorescence/Raman method with high levels of success on CBE materials.

The next generation instruments are rapidly evolving beyond the ability to simply demonstrate detection capability but designed to operate within a use-scenario of the warfighter, checkpoint system, or alternative ConOps. However in all of these scenarios what is unclear is how the operator searches for a possible explosive. While in some cases there is a need to analyze a suspicious “white” powder, trace detection requires a means to find potential areas of interest. As such, in addition to enabling point detection, the next generation of instruments includes the ability to map an area to provide the operator a means to find “hot spots”. This is currently not possible with the current Raman methods as the integration time/point is too lengthy for any implementation other than on a stable platform/microscope stage. Native fluorescence however can operate at the 60 - 100 μ s/point to rapidly create a map of larger areas to find potential “hot spots”. Those areas can then be further investigated using the deep UV Raman point analysis. Fortunately, both these capabilities can be incorporated into a single instrument; an example of this in a compact functional form is the SHERLOC (Scanning Habitable Environments with Raman and Luminescence for Organics and Chemicals) prototype shown in figure 3.1.B [64].

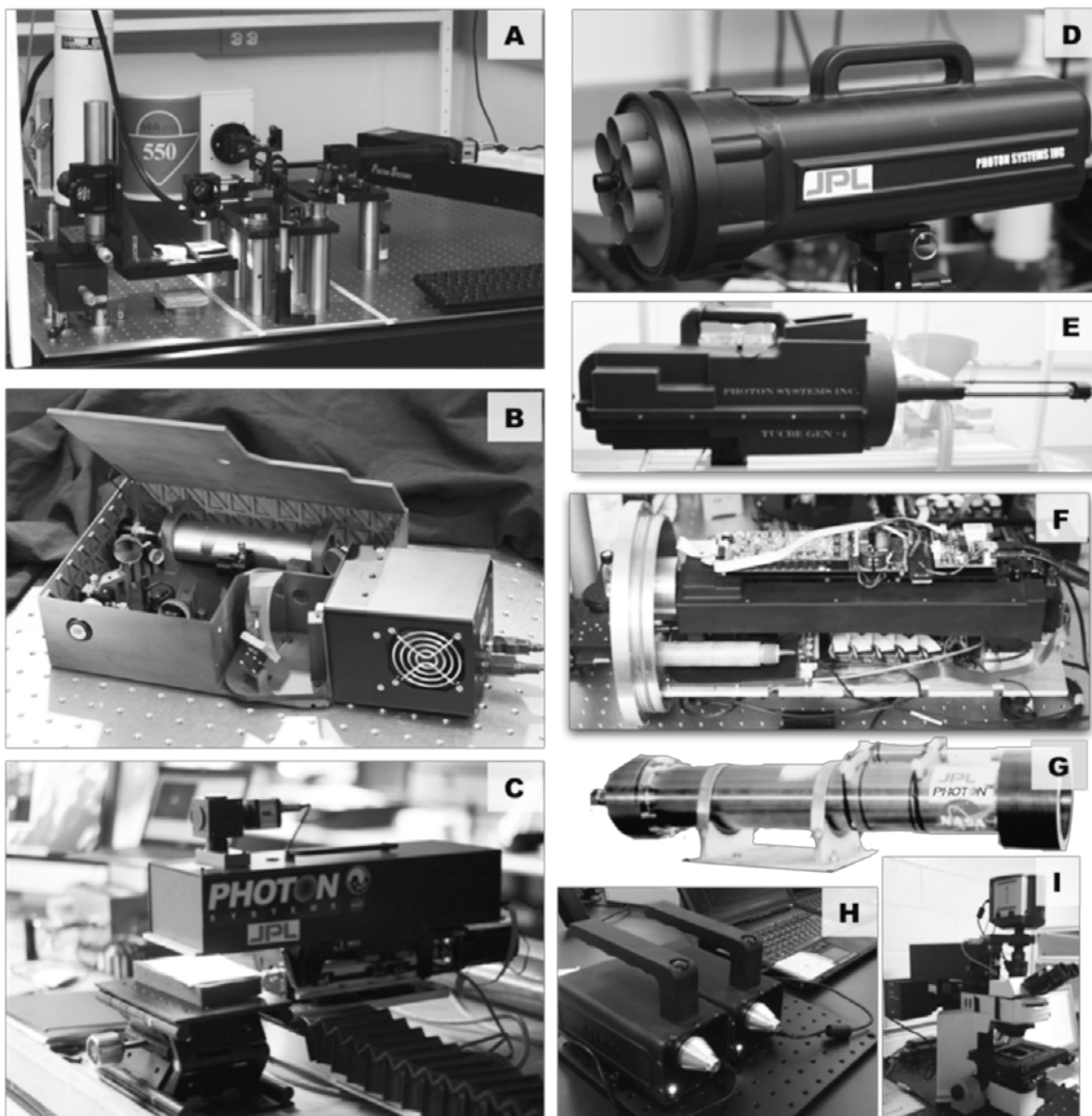


Figure 3.1. Examples of the Deep UV fluorescence/Raman instruments that have been developed since 1996. A) Deep UV Raman Fluorescence gold-standard MOBIUS - Mineralogy and Organic Based Investigations with UV Spectroscopy. **B)** Custom miniature deep UV Raman/fluorescence prototype (SHERLOC). DUV laser is the silver cylinder, **C)** MOSAIC – Microbial and Organics Surface Analyzer/Image Constructor, a macro-scale mapping fluorescence/Raman instrument, **D)** 1-2 m Standoff Deep UV fluorescence instrument, TUCBE Gen 2 sensor (Targeted Ultraviolet Chemical, Biological, Explosive sensor) **E)** 1-2 m standoff fluorescence/Raman instrument, TUCBE Gen 4.5, **F)** 100 m submersible deep UV fluorescence/Raman instrument for divers, SubCBE (Submersible Chemical, Biological, Explosives sensor), **G)** 5 km submersible DUV fluorescence instrument for hydrothermal vent analysis, DEBI-t (Dark Energy Biosphere Investigations Tool) **H)** Deep UV LED based fluorescence instruments for vapor and surface analysis (NaDos – Naphthalene DOSimeter), **I)** Deep UV fluorescence imaging microscope. microMOSAIC. DUV fluorescence/Raman instrument for scientific and DoD related applications have been commercially available since 2001.

- [1] S. Wallin, A. Pettersson, H. Östmark, and A. Hobro, "Laser-based standoff detection of explosives: a critical review," *Anal Bioanal Chem*, vol. 395, no. 2, pp. 259–274, May 2009.
- [2] M. K. McPherson, "Explosive Detection Equipment Program," *2010 IEEE International Carnahan Conference on Security Technology (ICCST)*, pp. 403–406, 2010.
- [3] D. S. Moore and R. J. Scharff, "Portable Raman explosives detection," *Anal Bioanal Chem*, vol. 393, no. 6, pp. 1571–1578, Mar. 2009.
- [4] D. D. Tuschel, A. V. Mikhonin, B. E. Lemoff, and S. A. Asher, "Deep Ultraviolet Resonance Raman Excitation Enables Explosives Detection," *Appl Spectrosc*, vol. 64, no. 4, pp. 425–432, Apr. 2010.
- [5] A. Blanco, L. C. Pacheco-Londoño, A. J. Peña-Quevedo, and S. P. Hernández-Rivera, "UV Raman detection of 2,4-DNT in contact with sand particles," *Detection and Remediation Technologies for Mines and Minelike Targets XI. Edited by Broach*, vol. 6217, pp. 100–621737–10, Jun. 2006.
- [6] W. F. Hug, R. D. Reid, R. Bhartia, and A. L. Lane, "A new miniature hand-held solar-blind reagentless standoff chemical, biological, and explosives (CBE) sensor," *Proc. SPIE*, vol. 6954, pp. 14–69540I–9, May 2008.
- [7] W. F. Hug, R. D. Reid, R. Bhartia, and A. L. Lane, "Performance status of a small robot-mounted or hand-held, solar-blind, standoff chemical, biological, and explosives (CBE) sensor," *Proc. SPIE*, vol. 7304, pp. 26–73040Z–8, May 2009.
- [8] R. Bhartia, W. F. Hug, and R. D. Reid, "Improved sensing using simultaneous deep UV Raman and fluorescence detection," *Proc. SPIE*, vol. 8358, pp. 35–83581A–9, May 2012.
- [9] D. S. Moore, "Recent Advances in Trace Explosives Detection Instrumentation," *Sens Imaging*, vol. 8, no. 1, pp. 9–38, May 2007.
- [10] M. Wu, M. Ray, K. Fung, M. Ruckman, D. Harder, and A. Sedlecek, "Stand-off detection of chemicals by UV Raman spectroscopy," *Appl Spectrosc*, vol. 54, 2000.
- [11] D. D. Tuschel, A. V. Mikhonin, B. E. Lemoff, and S. A. Asher, "Deep Ultraviolet Resonance Raman Spectroscopy of Explosives," presented at the XXII INTERNATIONAL CONFERENCE ON RAMAN SPECTROSCOPY. AIP Conference Proceedings, 2010, vol. 1267, pp. 869–870.
- [12] C. C. Phifer, R. L. Schmitt, L. R. Thorne, and P. Hargis Jr, *Studies of the laser-induced fluorescence of explosives and explosive compositions*. SAND2006-6697. Sandia National Laboratories, 2006.
- [13] M. Gaft and L. Nagli, "Standoff laser-based spectroscopy for explosives detection," *Electro-Optical Remote Sensing*, vol. 6739, pp. 2–673903–13, Oct. 2007.
- [14] R. Rumelfanger, S. A. Asher, and M. B. Perry, "UV resonance Raman characterization of polycyclic aromatic hydrocarbons in coal liquid distillates," *Appl Spectrosc*, vol. 42, no. 2, pp. 267–272, 1988.
- [15] C. M. Jones and S. A. Asher, "Ultraviolet resonance Raman study of the pyrene S₄, S₃, and S₂ excited electronic states," *The Journal of Chemical Physics*, vol. 89, no. 5, p. 2649, 1988.
- [16] S. A. Asher and C. R. Johnson, "Raman spectroscopy of a coal liquid shows that

- fluorescence interference is minimized with ultraviolet excitation.,” *Science*, vol. 225, no. 4659, pp. 311–313, Jul. 1984.
- [17] S. A. Asher, R. W. Bormett, X. G. Chen, D. H. Lemmon, N. Cho, P. Peterson, M. Arrigoni, L. Spinelli, and J. Cannon, “UV Resonance Raman Spectroscopy Using a New cw Laser Source: Convenience and Experimental Simplicity,” *Appl Spectrosc*, vol. 47, no. 5, pp. 628–633, 1993.
- [18] S. Asher and C. Johnson, “UV resonance Raman excitation profile through the 1B_{2u} state of benzene,” *The Journal of Physical Chemistry*, pp. 1375–1379, 1985.
- [19] C. Johnson and S. Asher, “UV resonance Raman excitation profiles of l-cystine,” *J. Raman Spectrosc.*, 1987.
- [20] S. Asher, M. Ludwig, and C. Johnson, “UV resonance Raman excitation profiles of the aromatic amino acids,” *Journal of the American Chemical Society*, vol. 108, no. 12, pp. 3186–3197.
- [21] S. A. Asher, “UV resonance Raman spectroscopy for analytical, physical, and biophysical chemistry,” *Anal. Chem.*, 1993.
- [22] S. A. Asher, “UV Resonance Raman Studies of Molecular Structure and Dynamics: Applications in Physical and Biophysical Chemistry,” *Annu. Rev. Phys. Chem.*, vol. 39, pp. 537–588, Oct. 1988.
- [23] S. A. Asher and J. L. Murtaugh, “UV Raman excitation profiles of imidazole, imidazolium, and water,” *Appl Spectrosc*, vol. 42, no. 1, pp. 83–90, Jan. 1988.
- [24] J. M. Dudik, C. R. Johnson, and S. A. Asher, “UV resonance Raman studies of acetone, acetamide, and N-methylacetamide: models for the peptide bond,” *The Journal of Physical Chemistry*, vol. 89, no. 18, pp. 3805–3814, Aug. 1985.
- [25] C. M. Jones, V. L. Devito, P. A. Harmon, and S. A. Asher, “High-Repetition-Rate Excimer-Based UV Laser Excitation Source Avoids Saturation in Resonance Raman Measurements of Tyrosinate and Pyrene,” *Appl Spectrosc*, vol. 41, no. 8, pp. 1268–1275, Nov. 1987.
- [26] J. M. Dudik, C. R. Johnson, and S. A. Asher, “Wavelength dependence of the preresonance Raman cross sections of CH₃CN, SO₄²⁻, ClO₄⁻, and NO₃⁻,” *The Journal of Chemical Physics*, vol. 82, no. 4, p. 1732, 1985.
- [27] W. F. Hug and R. D. Reid, “Apparatus for the efficient and accurate analysis of preferential compounds in sample,” U.S. Patent 6,287,869, 11-Sep-2001.
- [28] W. F. Hug and R. D. Reid, “Sputtering metal ion laser,” U.S. Patent 6,693,944, 17-Feb-2004.
- [29] W. F. Hug and R. D. Reid, “Spectroscopic chemical analysis methods and apparatus,” U.S. Patent 7,800,753, 21-Sep-2010.
- [30] W. F. Hug, R. D. Reid, and R. Bhartia, “Spectroscopic chemical analysis methods and apparatus,” U.S. Patent 8,395,770, 12-Mar-2013.
- [31] M. Storrie-Lombardi, W. Hug, G. McDonald, A. Tsapin, and K. Nealon, “Hollow cathode ion lasers for deep ultraviolet Raman spectroscopy and fluorescence imaging,” *Rev. Sci. Instrum.*, vol. 72, no. 4452, 2001.
- [32] X. Zhang and J. V. Sweedler, “Ultraviolet native fluorescence detection in capillary electrophoresis using a metal vapor NeCu laser,” *Anal. Chem.*, vol. 73, no. 22, pp. 5620–5624, 2001.
- [33] M. Sparrow, J. Jackovitz, C. Munro, W. Hug, and S. Asher, “New 224 nm

- Hollow Cathode Laser–UV Raman Spectrometer,” *Appl Spectrosc*, vol. 55, 2001.
- [34] A. U. Acuña, F. Amat-Guerri, P. Morcillo, M. Liras, and B. Rodríguez, “Structure and Formation of the Fluorescent Compound of *Lignum nephriticum*,” *Org. Lett.*, vol. 11, no. 14, pp. 3020–3023, Jul. 2009.
- [35] R. Borkman and D. Kearns, “Electronic Relaxation Processes in Acetone,” *The Journal of Chemical Physics*, vol. 44, no. 945, 1966.
- [36] R. Bhartia, W. F. Hug, E. C. Salas, R. D. Reid, K. K. Sijapati, A. Tsapin, W. Abbey, K. H. Nealon, A. L. Lane, and P. G. Conrad, “Classification of organic and biological materials with deep ultraviolet excitation,” *Appl Spectrosc*, vol. 62, no. 10, pp. 1070–1077, Oct. 2008.
- [37] J. Kim, F. Kim, and J. Huang, “Seeing graphene-based sheets,” *Materials Today*, vol. 13, no. 3, pp. 28–38, 2010.
- [38] K. Loh, Q. Bao, and G. Eda, “Graphene oxide as a chemically tunable platform for optical applications : Nature Chemistry : Nature Publishing Group,” *Nature Chemistry*, 2010.
- [39] N. Tarcea, T. Frosch, P. Rosch, M. Hilchenbach, T. Stuffer, S. Hofer, H. Thiele, R. Hochleitner, and J. Popp, “Raman Spectroscopy—A Powerful Tool for in situ Planetary Science,” *Space Science Reviews*, vol. 135, no. 1, pp. 281–292, Mar. 2008.
- [40] T. Frosch, N. Tarcea, M. Schmitt, H. Thiele, F. Langenhorst, and J. Popp, “UV Raman imaging—a promising tool for astrobiology: comparative Raman studies with different excitation wavelengths on SNC Martian meteorites,” *Anal. Chem.*, vol. 79, no. 3, pp. 1101–1108, Feb. 2007.
- [41] P. V. Johnson, R. Hodyss, D. K. Bolser, R. Bhartia, A. L. Lane, and I. Kanik, “Ultraviolet-stimulated fluorescence and phosphorescence of aromatic hydrocarbons in water ice,” *Astrobiology*, vol. 11, no. 2, pp. 151–156, Mar. 2011.
- [42] J. L. Anderson, A. A. Cantu, A. W. Chow, P. S. Fussell, R. G. Nuzzo, J. E. Parmeter, G. S. Saylor, J. M. Shreeve, R. E. Slusher, and M. Story, *Existing and Potential Standoff Explosives Detection Techniques*. The National Academies Press, 2004.
- [43] P. L. Marinkas, “Luminescence Properties of RDX and HMX,” Aug. 1975.
- [44] C. C. Phifer, R. L. Schmitt, L. R. Thorne, and P. Hargis Jr, *Studies of the laser-induced fluorescence of explosives and explosive compositions*. SAND2006-6697. Sandia National Laboratories, 2006.
- [45] C. Capellos, P. Papagiannakopoulos, and Y. Liang, “The 248 nm photodecomposition of hexahydro-1, 3, 5-trinitro-1, 3, 5-triazine,” *Chemical Physics Letters*, 1989.
- [46] P. L. Marinkas, “Luminescence of solid cyclic polynitramines,” *Journal of Luminescence*, vol. 15, no. 1, pp. 57–67, Mar. 1977.
- [47] K. Katoh, S. Yoshino, S. Kubota, Y. Wada, Y. Ogata, M. Nakahama, S. Kawaguchi, and M. Arai, “The Effects of Conventional Stabilizers and Phenol Compounds Used as Antioxidants on the Stabilization of Nitrocellulose,” *Prop., Explos., Pyrotech.*, vol. 32, no. 4, pp. 314–321, Aug. 2007.
- [48] L. Brus and J. McDonald, “Collision free, time resolved fluorescence of SO₂ excited near 2900 Å,” *Chemical Physics Letters*, 1973.

- [49] M. C. Thurber and R. K. Hanson, "Pressure and composition dependences of acetone laser-induced fluorescence with excitation at 248, 266, and 308 nm," *Applied Physics B*, vol. 69, no. 3, pp. 229–240, 1999.
- [50] R. Bhartia, W. F. Hug, E. C. Salas, K. Sijapati, A. L. Lane, R. D. Reid, and P. G. Conrad, "Biochemical detection and identification false alarm rate dependence on wavelength using laser induced native fluorescence," *Chemical and Biological Sensing VII. Edited by Gardner*, vol. 6218, pp. 17–62180J–9, Jun. 2006.
- [51] D. A. Skoog, F. J. Holler, and S. R. Crouch, *Principles of instrumental analysis*. Brooks/Cole Pub Co, 2007.
- [52] C. V. Raman and K. S. Krishnan, "Molecular Spectra in the Extreme Infra-Red," *Nature*, vol. 122, no. 3069, pp. 278–278, Aug. 1928.
- [53] M. J. Pelletier, *Analytical applications of Raman spectroscopy*. Wiley-Blackwell, 1999.
- [54] E. Ghiamati, R. Manoharan, W. Nelson, and J. Sperry, "UV Resonance Raman Spectra of Bacillus Spores," *Appl Spectrosc*, vol. 46, 1992.
- [55] N. Tarcea, M. Harz, P. Rösch, T. Frosch, M. Schmitt, H. Thiele, R. Hochleitner, and J. Popp, "UV Raman spectroscopy--a technique for biological and mineralogical in situ planetary studies.," *Spectrochimica Acta Part A: Molecular and Biomolecular Spectroscopy*, vol. 68, no. 4, pp. 1029–1035, Dec. 2007.
- [56] D.-Y. Wu, X.-M. Liu, S. Duan, X. Xu, B. Ren, S.-H. Lin, and Z.-Q. Tian, "Chemical Enhancement Effects in SERS Spectra: A Quantum Chemical Study of Pyridine Interacting with Copper, Silver, Gold and Platinum Metals," *J. Phys. Chem. C*, vol. 112, no. 11, pp. 4195–4204, Mar. 2008.
- [57] M. Ghosh, L. Wang, and S. A. Asher, "Deep-Ultraviolet Resonance Raman Excitation Profiles of NH₄NO₃, PETN, TNT, HMX, and RDX," *Appl Spectrosc*, vol. 66, no. 9, pp. 1013–1021, Sep. 2012.
- [58] M. Gaft and L. Nagli, "UV gated Raman spectroscopy for standoff detection of explosives," *Optical Materials*, vol. 30, no. 11, pp. 1739–1746, 2008.
- [59] A. Ehlerding, I. Johansson, S. Wallin, and H. Östmark, "Resonance-Enhanced Raman Spectroscopy on Explosives Vapor at Standoff Distances," *International Journal of Spectroscopy*, vol. 2012, no. 3, pp. 1–9, 2012.
- [60] A. Tripathi, E. D. Emmons, P. G. Wilcox, J. A. Guicheteau, D. K. Emge, S. D. Christesen, and A. W. Fountain III, "Semi-Automated Detection of Trace Explosives in Fingerprints on Strongly Interfering Surfaces with Raman Chemical Imaging," *Appl Spectrosc*, vol. 65, no. 6, pp. 611–619, Jun. 2011.
- [61] G. H. Peters, W. Abbey, G. H. Bearman, G. S. Mungas, J. A. Smith, R. C. Anderson, S. Douglas, and L. W. Beegle, "Mojave Mars simulant—Characterization of a new geologic Mars analog," *Icarus*, vol. 197, no. 2, pp. 470–479, Oct. 2008.
- [62] G. Mallocci, G. Mulas, and C. Joblin, "Electronic absorption spectra of PAHs up to vacuum UV. Towards a detailed model of interstellar PAH photophysics," *A&A*, vol. 426, no. 1, pp. 105–117, Oct. 2004.
- [63] N. Gomer, C. Gordon, P. Lucey, S. Sharma, J. Carter, and S. Angel, "Raman Spectroscopy Using a Spatial Heterodyne Spectrometer: Proof of Concept," *Appl Spectrosc*, vol. 65, 2011.

- [64] L. W. Beegle, R. Bhartia, L. DeFlores, M. Darrach, R. D. Kidd, W. Abbey, S. Asher, A. Burton, S. Clegg, P. G. Conrad, K. Edgett, B. Ehlmann, F. Langenhorst, M. Fries, W. Hug, K. Neelson, J. Popp, P. Sorbon, A. Steele, R. Wiens, and K. Williford, "SHERLOC: Scanning Habitable Environments with Raman and Luminescence for Organics and Chemicals, an Investigation for 2020," *Lunar and Planetary Institute Science Conference Abstracts*, vol. 45, p. 2835, Mar. 2014.